CrossMark

ORIGINAL PAPER

Comparison of the Oxidation Process in Pure Iron and Diluted Fe–Si Alloys: A Transmission Mössbauer Spectroscopy Study

R. Idczak[1]

Abstract The room temperature study of polycrystalline iron, $Fe_{0.99}Si_{0.01}$ and $Fe_{0.97}Si_{0.03}$ alloys, was performed using the ^{57}Fe transmission Mössbauer spectroscopy (TMS). The TMS measurements allow us to determine changes of chemical composition and content of iron oxides in the studied samples during exposure to air at 570, 870 and 1070 K. The results indicate that the chemical composition of samples changes significantly and it is strongly dependent on the temperature at which the studied samples are exposed to air. Moreover, it was shown that the addition of few atomic percent of Si impurities to iron leads to a significant slowdown of the internal oxidation process. The iron and silicon internal oxidation kinetics for $Fe_{0.99}Si_{0.01}$ and $Fe_{0.97}Si_{0.03}$ alloys were calculated using the Deal-Grove model. The activation energies E_A for the internal oxidation of iron atoms in studied Fe–Si alloys were estimated: $E_A = 1.46$ (3) eV for $Fe_{0.99}Si_{0.01}$ and $E_A = 1.62$ (6) eV for $Fe_{0.97}Si_{0.03}$.

Keywords Mössbauer spectroscopy · Polycrystalline iron · Iron alloys · High-temperature corrosion · Internal oxidation

Introduction

Corrosion of iron has been intensively studied for years due to the fact that iron as well as their alloys is still one of the most important construction materials for the modern industry, and their inevitable contact with oxygen (atmospheric for instance) often leads to changes in their mechanical, magnetic, structural and

✉ R. Idczak
  ridczak@ifd.uni.wroc.pl

[1] Institute of Experimental Physics, University of Wrocław, pl. M. Borna 9, 50-204 Wrocław, Poland

thermodynamic properties [1–6]. The oxidation behaviour of Fe–Si alloys at high temperatures in different atmospheres has been investigated by several researchers [7–11]. One of the main conclusions which comes from these works is that the addition of silicon has a significant effect on the oxidation resistance of iron in O_2 or in air up to 1300 K. In this work, the polycrystalline iron and $Fe_{0.99}Si_{0.01}$ and $Fe_{0.97}Si_{0.03}$ alloys, which were exposed to air at 570 K, 870 K and 1070 K, were investigated using the [57]Fe transmission Mössbauer spectroscopy (TMS). These measurements allowed the comparison of the oxidation process in three different materials under the same oxidation conditions. Base on TMS data, it is possible to calculate the iron and silicon internal oxidation kinetics and the activation energies for the internal oxidation of iron atoms in studied Fe–Si alloys.

Experimental Procedures

Samples of pure Fe (99.98 %) were prepared by iron rod cold-rolling to the final thickness of about 0.035 mm. At the same time, the samples of $Fe_{0.99}Si_{0.01}$ and $Fe_{0.97}Si_{0.03}$ alloys were prepared in an arc furnace. Appropriate amounts of the 99.98 % pure iron and 99.95 % pure silicon were melted into a water-cooled copper crucible in argon atmosphere and then quickly cooled to room temperature. Solidified alloys were remelted twice to ensure homogeneity. The weight losses during the melting process were below 0.2 % of the original weight, so the compositions of the obtained ingots were close to the nominal ones. Resulting ingots were cold-rolled to the final thickness of about 0.035 mm. In the next step, iron and $Fe_{0.99}Si_{0.01}$ and $Fe_{0.97}Si_{0.03}$ foils were annealed in the vacuum at 1270 K for 2 h. The base pressure during the annealing procedure was lower than 10^{-6} mbar. To obtain homogeneous and defect-free samples [12], after annealing process, the foils were slowly cooled to room temperature for 6 h. The annealed samples were exposed to air at 570, 870 and 1070 K for several hours. Each step of the sample processing was followed by TMS measurements, which were performed at room temperature by means of a constant-acceleration POLON spectrometer of standard design, using a 3.7 GBq [57]Co-in-Rh standard source with a full width at half maximum (FWHM) of 0.22 mm/s. Each measured TMS spectrum was analysed in terms of a sum of different number of single lines and six-line patterns, corresponding to various isomer shifts *IS*, quadrupole splitting *QS* and hyperfine fields *B* at [57]Fe nuclei generated by different chemical states of [57]Fe Mössbauer probes. The fitting procedure was done under the thin absorber approximation, and it was assumed that the shape of each line could be fitted by Voigt function (the convolution on Lorentzian and Gaussian curves). For each six-line pattern, the two-line area ratio I_{16}/I_{34} is constant and equal to 3/1. The ratio I_{25}/I_{34} and three linewidths Γ_{16}, Γ_{25} and Γ_{34} are free parameters. Some of the obtained fits are shown in Figs. 1, 2, 3 and 4.
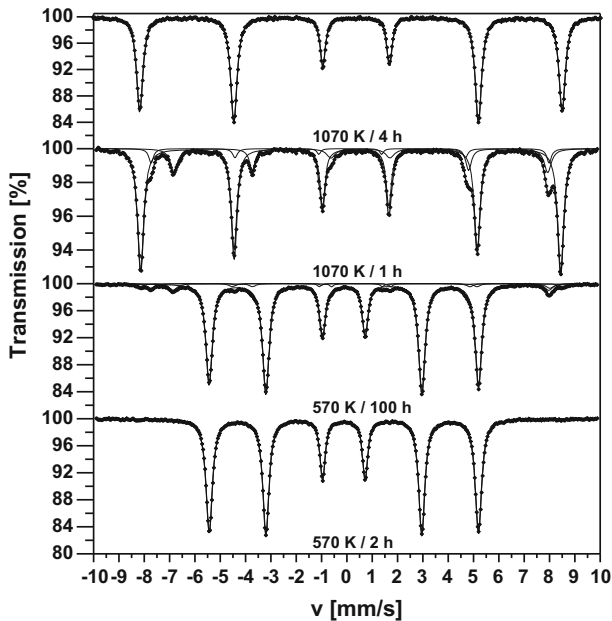
Fig. 1 The room-temperature TMS spectra of the Fe sample exposed to air at 570 and 1070 K for several hours h, fitted with a sum of various numbers of *six-line* patterns corresponding to different chemical states of iron atoms

Results and Discussion

Results for Pure Iron

As one can see in Figs. 1 and 2, the measured TMS spectra for pure iron samples change significantly with exposure to air. For samples exposed to air at 570 K for 2 and 16 h, each spectrum can be described with one six-line pattern only having the hyperfine parameters similar to those for metallic iron with b.c.c. structure (α-Fe). At longer exposure times (40 and 100 h), the additional magnetically splitted components were observed. These subspectra were accounted for by adding to the model of the spectrum three sextets. The estimated, during fitting procedure, hyperfine parameters for the samples mentioned above correspond to α-iron and two different iron oxides. One sextet with B ≈ 51.7 T, IS ≈ 0.37 mm/s and QS ≈ −0.2 mm/s could be a result of the α-Fe_2O_3 presence in the sample [13]. The last two sextets with B ≈ 48.9 and 46.1 T, IS ≈ 0.24 mm/s and 0.68 mm/s and QS < 0.1 mm/s correspond to the two different sites of Fe atoms in Fe_3O_4 compound [14]. At higher temperatures (870 and 1070 K), the obtained spectra consist of a various number of sextets which correspond to the existence of α-Fe and α-Fe_2O_3 and Fe_3O_4 compounds. Here it is worth noting that changes in relative intensities of two Fe_3O_4 sextets were observed. This fact suggests that stoichiometric and non-stoichiometric Fe_3O_4 were formed [15, 16]. Moreover, in spectra obtained for iron exposed to air at 870 K for 2 and 4 h, the additional non-magnetic
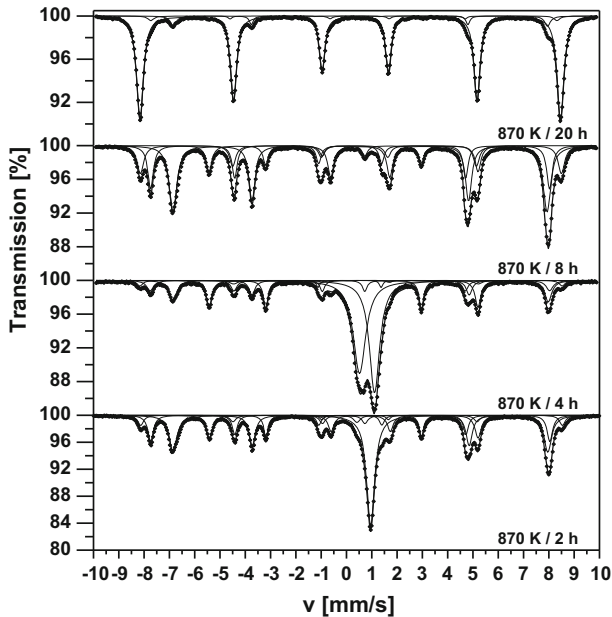
Fig. 2 The room-temperature TMS spectra of the Fe sample exposed to air at 870 K for several hours h, fitted with a sum of various numbers of *single lines* and *six-line* patterns corresponding to different chemical states of iron atoms

components were observed. Two singlets with IS $\approx$ 1.05 and 0.55 mm/s could be assigned to stoichiometric and non-stoichiometric FeO [17]. At the same time, in all measured TMS spectra, there are no other components which could be connected with FeOOH or iron carbides [18, 19]. The above findings are important evidence that in polycrystalline Fe exposed to air at elevated temperatures, only three types of compounds are formed: FeO, α-Fe_2O_3 and Fe_3O_4. Moreover, as a result of the analysis, the relative areas I(x) of components for each spectrum were determined. Assuming that the relative ratio of the Lamb–Mössbauer factors $f_{\alpha\text{-Fe}}$: f_{FeO}: $f_{\alpha\text{-Fe2O3}}$: f_{Fe3O4} is equal to 1: 1: 1.08: 1.05 [1], the fraction $c(x)$ of absorbing atoms corresponding to each component can be easily calculated using the I(x) values as follows:

$$c(x) = \frac{I(x)}{\sum I(x)} \tag{1}$$

The computed c(x) values were used to find parameters c(Fe), c(FeO), c(Fe_2O_3) and c(Fe_3O_4) which are the total intensities of spectrum components related to the existence of ^{57}Fe nuclear probes in α-Fe, FeO, α-Fe_2O_3 and Fe_3O_4, respectively. These parameters are listed in Table 1. Finally, to obtain the chemical composition of studied samples, it is necessary to taking into account that the relative quantities of iron atoms in observed compounds are different and equal to 1: 1: 2: 3 for α-Fe, FeO, α-Fe_2O_3 and Fe_3O_4, respectively. The chemical
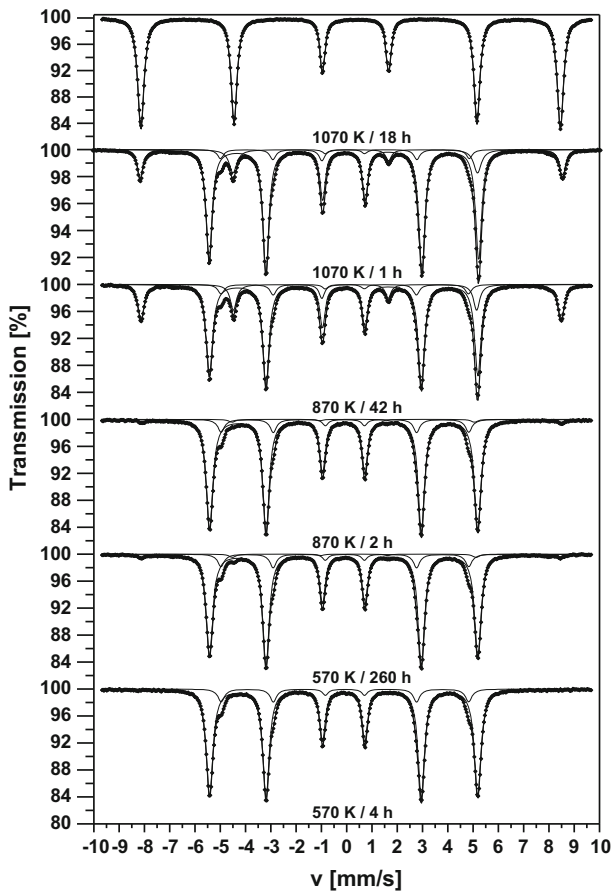
Fig. 3 The room-temperature TMS spectra of the $Fe_{0.99}Si_{0.01}$ sample exposed to air at 570, 870 and 1070 K for several hours h, fitted with a sum of various numbers of *six-line* patterns corresponding to different chemical states of iron atoms

composition estimated under the above-mentioned assumptions is shown in Fig. 5. The data show that exposure of polycrystalline iron to air at elevated temperatures results in the formation of three different iron oxides, which are quite similar to those obtained in previous works concerning the oxidation of iron in air [5].

Results for $Fe_{0.99}Si_{0.01}$ and $Fe_{0.97}Si_{0.03}$ Alloys

The TMS spectra analysis revealed the existence of components which could be assigned to single-phase Fe–Si alloy with b.c.c. structure [20], α-Fe_2O_3 and stoichiometric and non-stoichiometric Fe_3O_4 compounds with hyperfine parameters similar to those obtained for pure iron spectra. In the next step, based on the procedure proposed in Sect. 3.1, the total intensities of TMS spectrum components c(alloy), c(Fe_2O_3) and c(Fe_3O_4) and the chemical composition for the studied alloys were calculated (Tables 2, 3 and Fig. 5).
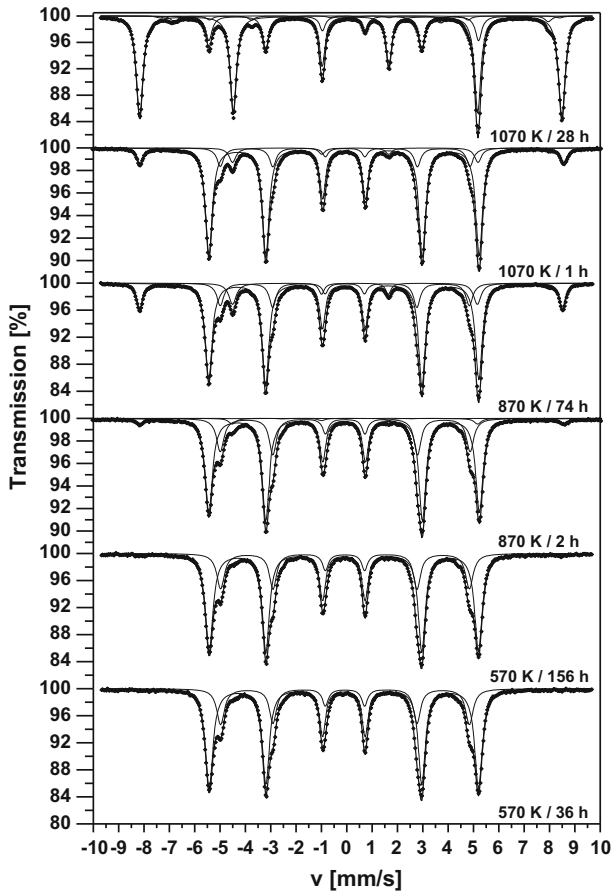
Fig. 4 The room-temperature TMS spectra of the $Fe_{0.97}Si_{0.03}$ sample exposed to air at 570, 870 and 1070 K for several hours h, fitted with a sum of various numbers of *six-line* patterns corresponding to different chemical states of iron atoms

As one can expect, a few atomic percent of Si impurities dissolved in the iron matrix have a significant influence on oxidation process of iron atoms in studied materials. Firstly, in contrast to pure iron oxidation where exposure to air at elevated temperatures results in the formation of three different iron oxides, in Fe–Si alloys the dominant type of iron oxide is Fe_2O_3. FeO does not form at all and the intensity of Fe_3O_4 component in measured spectra does not exceed 5 %. Secondly, the comparison of data, as presented in Tables 1, 2 and 3 leads to a conclusion that the internal oxidation of iron atoms slows with increasing Si content.

Oxidation Kinetics and Activation Energy

To analyse thermal oxidation of iron in Fe–Si alloys, the Deal–Grove model was applied [21]. This model requires that the oxidation of Fe follows a mechanism
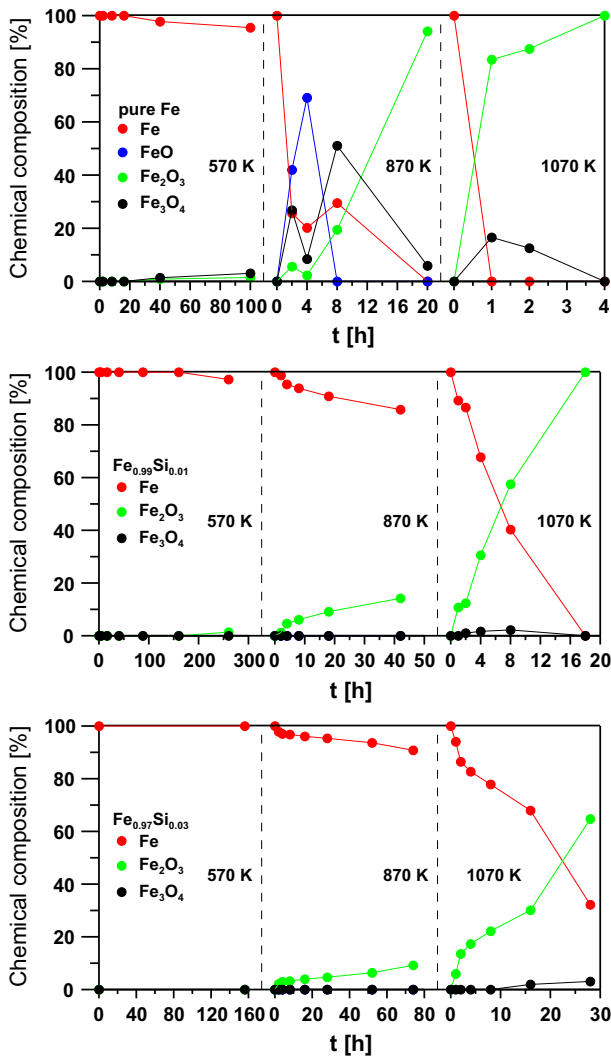
Fig. 5 The chemical composition of Fe, $Fe_{0.99}Si_{0.01}$ and $Fe_{0.97}Si_{0.03}$ samples exposed to air at 570, 870 and 1070 K as a function of exposure time. The standard uncertainties for the presented quantities do not exceed 3 %

whereby a thin layer of oxide is formed by place exchange after adsorption has occurred, with further oxidation occurring due to an electric field mechanism. The electric field is formed by electrons tunnelling from the metal to the adsorbed oxygen, and is able to support ion transport through the place exchange and formed thin oxide layer enabling the oxide layer to increase in thickness. Due to the fact that TMS technique is not sensitive to thin oxide layer (below 100 nm), the parabolic regime (for thick films) was applied:

Table 1 TMS measurements of total intensities of components which are related to the existence of ^{57}Fe nuclear probes in α-Fe, FeO, α-Fe$_2$O$_3$ and Fe$_3$O$_4$

Exposure time (h)	c(Fe) (%)	c(FeO) (%)	c(Fe$_2$O$_3$) (%)	c(Fe$_3$O$_4$) (%)
570 K				
2	100	0	0	0
8	100	0	0	0
16	100	0	0	0
40	94	0	2	4
100	89	0	3	8
870 K				
2	16	27	7	50
4	17	58	4	21
8	13	0	18	69
20	0	0	91	9
1070 K				
1	0	0	77	23
2	0	0	82	18
4	0	0	100	0

The standard uncertainties for the $c(x)$ parameters do not exceed 1 %

Table 2 TMS measurements of total intensities of components which are related to the existence of ^{57}Fe nuclear probes in Fe$_{0.99}$Si$_{0.01}$ alloy, α-Fe$_2$O$_3$ and Fe$_3$O$_4$

Exposure time (h)	c(alloy) (%)	c(Fe$_2$O$_3$) (%)	c(Fe$_3$O$_4$) (%)
570 K			
4	100	0	0
16	100	0	0
40	100	0	0
88	100	0	0
160	100	0	0
260	97	3	0
870 K			
2	98	2	0
4	91	9	0
8	89	11	0
18	83	17	0
42	75	25	0
1070 K			
1	81	19	0
2	76	22	2
4	51	46	3
8	25	71	4
18	0	100	0

The standard uncertainties for the $c(x)$ parameters do not exceed 1 %

Table 3 TMS measurements of total intensities of components which are related to the existence of ^{57}Fe nuclear probes in $Fe_{0.97}Si_{0.03}$ alloy, α-Fe_2O_3 and Fe_3O_4

Exposure time (h)	c(alloy) (%)	c(Fe$_2$O$_3$) (%)	c(Fe$_3$O$_4$) (%)
570 K			
2	100	0	0
12	100	0	0
36	100	0	0
84	100	0	0
156	100	0	0
870 K			
2	96	4	0
4	94	6	0
8	94	6	0
16	92	8	0
28	91	9	0
52	88	12	0
74	83	17	0
1070 K			
1	89	11	0
2	76	24	0
4	70	30	0
8	64	36	0
16	51	45	4
28	19	76	5

The standard uncertainties for the c(x) parameters do not exceed 1 %

Table 4 The estimated quadratic reaction rate constants k and activation energies of iron oxidation process E_A for studied Fe–Si alloys

T (K)	k (h^{-1})	E_A (eV)	E_A (kJ/mol)
Fe$_{0.99}$Si$_{0.01}$			
870	1.49×10^{-3}	1.46 (3)	141 (3)
1070	57.2×10^{-3}		
Fe$_{0.97}$Si$_{0.03}$			
870	0.35×10^{-3}	1.62 (6)	156 (6)
1070	19.9×10^{-3}		

The standard uncertainties for the k parameters do not exceed 10^{-4} h^{-1}

$$Fe_{OX}(t) = \sqrt{kt} \qquad (2)$$

where Fe_{OX} is a fraction of oxidised iron atoms in studied alloys at time t, and k denotes the quadratic reaction rate constant which is expressed as follows:

$$k = k_0 \exp\left(\frac{E_A}{k_B T}\right), \qquad (3)$$

where E_A is activation energy for iron oxidation, k_B stands for Boltzmann constant, k_0 is pre-exponential factor and T denotes temperature. The parabolic iron oxidation kinetic curves obtained for the $Fe_{0.99}Si_{0.01}$ and $Fe_{0.97}Si_{0.03}$ alloys exposed to air at 870 K and 1070 K, respectively, are shown in Fig. 6. The knowledge of the reaction rate k for two different temperatures, $T_1 = 870$ K and $T_2 = 1070$ K, combined with Eq. (3) enabled the determination of the activation energy E_A for the oxidation of iron atoms in the temperature interval of 870–1070 K, using the following equation:

$$E_A = \frac{T_1 T_2}{T_2 - T_1} k_B \ln\left(\frac{k_2}{k_1}\right). \tag{4}$$

This equation is valid assuming the pre-exponent factor k_0 in Eq. (3) is temperature independent. The estimated quadratic reaction rate constants and activation energies of iron oxidation process for studied Fe–Si alloys were presented in Table 4. The obtained E_A values for Fe–Si alloys are much higher compared to the activation energy for the oxidation reaction of pure Fe, which was determined to be 32 (6) kJ/mol [22]. This is in accord with the observation that the iron oxidation
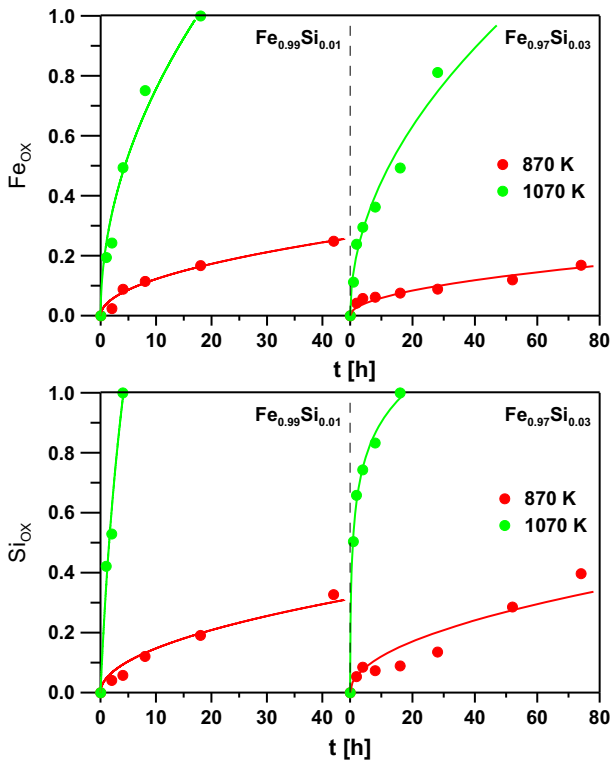

Fig. 6 The parabolic iron oxidation kinetics and the parabolic (for 870 K) and logarithmic (for 1070 K) silicon oxidation kinetics obtained for the $Fe_{0.99}Si_{0.01}$ and $Fe_{0.97}Si_{0.03}$ alloys exposed to air at 870 and 1070 K. The best fit to the data in terms of Eqs. (2 and 6) is indicated by *solid lines*

process in Fe–Si alloys was much slower compared to the one in pure iron sample. Moreover, the higher E_A value for $Fe_{0.97}Si_{0.03}$ alloy also agrees with the previous conclusion that the internal oxidation of iron atoms slows with increasing Si content.

Indirect Observation of Si Oxidation Process

The Si oxidation process cannot be directly observed using the [57]Fe Mössbauer spectroscopy. This is because this technique is not sensitive to presence of Si oxides in measured samples. Taking this into account, the indirect method for the above-mentioned observation is proposed. The analysis of TMS spectra, obtained for the $Fe_{0.99}Si_{0.01}$ and $Fe_{0.97}Si_{0.03}$ samples, reveals the existence of two components (sextets) which could be assigned to single-phase Fe–Si alloy with b.c.c. structure. The first sextet (the iron component), with $B \approx 32.9$ T and $IS \approx 0.00$ mm/s, corresponds to the presence of Fe atoms without any Si atoms in their first coordination shell. The second one (the satellite component), with $B \approx 30.5$ T and $IS \approx 0.05$ mm/s, corresponds to Fe atoms with one Si atom in their first coordination shell [20]. Assuming that the single-phase Fe–Si alloy with b.c.c. structure is quite homogenous and in annealed alloys, before exposure to air, all Si atoms are dissolved in iron matrix, it is possible to calculate atomic concentration of Si atoms c_{Si} which are not oxidised and located in the single-phase Fe–Si alloy as follows:

$$c_{Si} = 100\,\% \cdot \frac{I\,(\text{satellite})}{I\,(\text{iron}) + I\,(\text{satellite})} \Big/ Z, \tag{5}$$

where I(iron) and I(satellite) denote the intensities of the iron and the satellite components, respectively. Z is the first coordination number which for b.c.c. structure is equal to 8. The obtained values presented in Table 5 show a slight decrease of Si concentration in single-phase Fe–Si alloy during exposure to air. Having in mind that the [57]Fe Mössbauer spectroscopy is not sensitive to the presence of Si oxides, this result could be explained by faster oxidation of Si atoms in studied Fe–Si alloys. In other words, the oxygen atoms which diffuse into Fe–Si matrix at elevated temperatures prefer to form silicon oxides, and after their formation these compound cannot be directly observed using [57]Fe Mössbauer spectroscopy. This observation combined with the results obtained in Sects. 3.2 and 3.3 could give an answer as to why the addition of a few atomic percent of Si impurities to iron leads to a significant slowdown of the internal oxidation process. The most plausible explanation of this phenomenon is connected with the surface segregation process of Si atoms in Fe–Si alloys. An increased concentration of Si atoms on the surface of grains in polycrystalline Fe–Si alloy could form a stable silicon oxide passivation layer which significantly slows down the internal oxidation process. The segregation of Si on Fe–Si alloy surface was reported in several papers [23–25]. Unfortunately, due to the fact that these studies were performed on single crystal, it is necessary to confirm the segregation process in polycrystalline Fe–Si alloys.

Table 5 The estimated atomic concentration of Si atoms dissolved in the single-phase Fe–Si alloy with b.c.c. structure

Fe$_{0.99}$Si$_{0.01}$ (870 K)		Fe$_{0.99}$Si$_{0.01}$ (1070 K)		Fe$_{0.97}$Si$_{0.03}$ (870 K)		Fe$_{0.97}$Si$_{0.03}$ (1070 K)	
t (h)	c_{Si} (%)	t (h)	c_{Si} (%)	t (h)	c_{Si} (%)	t (h)	c_{Si} (%)
0	1.0	0	1.0	0	3.1	0	3.1
2	1.0	1	0.6	2	3.0	1	1.5
4	1.0	2	0.5	4	3.0	2	1.2
8	1.0	4	0	8	2.9	4	0.9
18	0.9	8	0	16	2.9	8	0.5
42	0.8			28	2.8	16	0
				52	2.4	28	0
				74	2.1		

The standard uncertainties for the c_{Si} values do not exceed 0.2 %

In the next step, using Eq. (1), the fraction of iron atoms with one Si impurity in their first coordination shell c(satellite) was computed. These values give information about the fraction of Si atoms which are not oxidised (dissolved in iron matrix), and 1-c(satellite) values denote the fraction of oxidised silicon atoms Si$_{OX}$. The obtained Si$_{OX}$ values for Fe$_{0.99}$Si$_{0.01}$ and Fe$_{0.97}$Si$_{0.03}$ samples as a function of exposure time are shown in Fig. 6. These results were used to estimate the parabolic iron oxidation kinetic curves for studied alloys which were exposed to air at 870 K. The computed quadratic reaction rate constants are $k = 2.17$ (5) 10^{-3} h^{-1} for Fe$_{0.99}$Si$_{0.01}$ and $k = 1.45$ (3) 10^{-3} h^{-1} for Fe$_{0.97}$Si$_{0.03}$. During analysis of the silicon oxidation kinetic curves, it was found that parabolic regime is not valid for samples oxidised at 1070 K. In that case, the logarithmic oxidation kinetics was much more plausible:

$$Si_{OX}(t) = k \cdot \log(Ct + 1) \tag{6}$$

where k denotes a logarithmic reaction rate constant and C is a constant. The computed logarithmic rate constants are $k = 2.2(9)$ for Fe$_{0.99}$Si$_{0.01}$ and $k = 0.39$ (3) for Fe$_{0.97}$Si$_{0.03}$. This result suggests that in diluted Fe–Si alloys, the silicon oxidation mechanism could be temperature-dependent.

Conclusions

The results reported in this paper can be concluded as follows:

1. The TMS measurements of pure iron and Fe$_{0.99}$Si$_{0.01}$ and Fe$_{0.97}$Si$_{0.03}$ alloys allowed us to determine changes of chemical composition and the presence of newly formed compounds in studied materials during exposure to air at 570, 870 and 1070 K.

2. As it was shown, a few atomic percent of Si impurities dissolved in the iron matrix have a significant influence on oxidation process of iron atoms in studied materials. In contrast to pure iron oxidation where exposure to air at elevated temperatures results in the formation of three different iron oxides, in Fe–Si alloys the dominant type of iron oxide is Fe_2O_3. FeO does not form at all and the intensity of Fe_3O_4 component in measured spectra does not exceed 5 %.
3. The comparison of data obtained for pure iron and $Fe_{0.99}Si_{0.01}$ and $Fe_{0.97}Si_{0.03}$ leads to a conclusion that the internal oxidation of iron atoms slows with increasing of Si content.
4. The estimation of the reaction rate k for two different temperatures, $T_1 = 870$ K and $T_2 = 1070$ K, enabled the determination of the activation energy E_A for the internal oxidation of iron atoms in studied Fe–Si alloys: $E_A = 1.46$ (3) eV for $Fe_{0.99}Si_{0.01}$ and $E_A = 1.62$ (6) eV for $Fe_{0.97}Si_{0.03}$.
5. The indirect observation of Si oxidation process in studied materials was proposed. Using this, the silicon oxidation kinetics for $Fe_{0.99}Si_{0.01}$ and $Fe_{0.97}Si_{0.03}$ alloys were presented. The obtained kinetics suggest that in diluted Fe–Si alloys, the silicon oxidation mechanism could be temperature-dependent.

References

1. D. A. Channing and M. J. Graham, *Corrosion Science* **12**, 1972 (271–289).
2. D. A. Channing, S. M. Dickerson and M. J. Graham, *Corrosion Science* **13**, 1973 (933–938).
3. A. P. Grosvenor, B. A. Kobe and N. S. McIntyre, *Surface Science* **565**, 2004 (151–162).
4. C. Han, C. Zhang, X. Liu, H. Huang, S. Zhuang, P. Han and X. Wu, *J Mol Model* **21**, 2015 (181).
5. K. Idczak, R. Idczak and R. Konieczny, *Physica B* **491**, 2016 (37–45).
6. K. Freindl, T. Ossowski, M. Zając, N. Spiridis, D. Wilgocka-Ślęzak, E. Madej, T. Giela, A. Kiejna and J. Korecki, *The Journal Of Physical Chemistry C* **120**, 2016 (3807–3813).
7. A. R. Lashin, O. Schneeweiss and Y. Houbaert, *Corrosion Science* **50**, 2008 (2580–2587).
8. M. A. A. Motin, J. Zhang, P. R. Munroe and D. J. Young, *Corrosion Science* **52**, 2010 (3280–3286).
9. H. Li, J. Zhang and D. J. Young, *Corrosion Science* **54**, 2012 (127–138).
10. A. R. Lashin, *Journal of Alloys and Compounds* **567**, 2013 (54–58).
11. L. L. Liu, Q. Q. Guo, S. Liu, C. S. Ni and Y. Niu, *Corrosion Science* **98**, 2015 (507–515).
12. R. Idczak, R. Konieczny and J. Chojcan, *Journal of Applied Physics* **115**, 2014 (103513).
13. R. Zboril, M. Mashlan and D. Petridis, *Chem. Mater.* **24**, 2002 (969–982).
14. B. J. Evans and S. S. Hafner, *Journal of Applied Physics* **40**, 1969 (1411–1413).
15. J. M. Daniels and A. Rosencwaig, *Journal of Physics and Chemistry of Solids* **30**, 1969 (1561–1571).
16. F. C. Voogt, T. Hibma, G. L. Zhang, M. Hoefman and L. Niesen, *Surface Science* **331–333**, 1995 (1508–1514).

17. L. F. Checherskaya, V. P. Romanov and P. A. Tatsienko, *Physica Status Solidi* **19**, 1973 (K177–K182).
18. F. Van der Woude and A. J. Dekker, *Physica Status Solidi* **13**, 1966 (181–193).
19. B. Kniep, A. Constantinescu, D. Niemeier and K. D. Becke, *Zeitschrift für Anorganische und Allgemeine Chemie* **629**, 2003 (1795–1804).
20. R. Idczak, R. Konieczny and J. Chojcan, *Acta Physica Polonica A* **129**, 2016 (367).
21. B. E. Deal and A. S. Grove, *Journal of Applied Physics* **36**, 1965 (3770–3778).
22. A. P. Grosvenor, B. A. Kobe and N. S. McIntyre, *Surface Science* **574**, 2005 (317–321).
23. J. Du Plessis and P. E. Viljoen, *Surface Science* **131**, 1983 (321–327).
24. H. De Rugy and H. Viefhaus, *Surface Science* **173**, 1986 (418–438).
25. P. Lejček, V. Paidar, S. A. Firstov, Yu N Ivashchenko and A. V. Krajnikov, *Scripta Metallurgica* **23**, 1989 (2147–2152).